Functional Models

Deutsche Ausgabe: DOI: 10.1002/ange.201607044
Internationale Ausgabe: DOI: 10.1002/anie.201607044

Mimicking the Aromatic-Ring-Cleavage Activity of Gentisate-1,2-Dioxygenase by a Nonheme Iron Complex

*Rubina Rahaman, Biswarup Chakraborty, and Tapan Kanti Paine**

Abstract: *Gentisate-1,2-dioxygenase (GDO), a nonheme iron enzyme in the cupin superfamily, catalyzes the cleavage of the aromatic-ring of 2,5-dihydroxybenzoic acid (gentisic acid) to form maleylpyruvic acid in the microbial aerobic degradation of aromatic compounds. To develop a functional model of GDO, we have isolated a nonheme iron(II) complex, [(Tp^{Ph2})Fe^{II}(DHN-H)] (Tp^{Ph2} = hydrotris(3,5-diphenylpyrazole-1-yl)borate, DHN-H = 1,4-dihydroxy-2-naphthoate). In the reaction with O_2, the biomimetic complex oxidatively cleaves the aromatic ring of the coordinated substrate with the incorporation of both the oxygen atoms from molecular oxygen into the cleavage product. The presence of para-hydroxy group on the substrate plays a crucial role in directing the aromatic-ring cleaving reaction.*

Bacterial nonheme iron enzymes catalyze a myriad of oxidative C–C bond cleavage reactions in the biodegradation of toxic and xenobiotic compounds.[1] The biodegradation process of aromatic compounds involves a number of intermediate compounds.[2] Gentisic acid (2,5-dihydroxybenzoic acid) is a key intermediate in the biodegradation of mono- and poly-cyclic aromatic, and hetero-aromatic compounds by microorganisms.[3,4] Gentisate-1,2-dioxygenase (GDO),[5–10] the nonheme iron enzyme isolated from a variety of sources, catalyzes the aromatic C–C bond cleavage of gentisate to form maleyl pyruvate using dioxygen as the oxidant (Scheme 1). The ring cleavage product maleyl

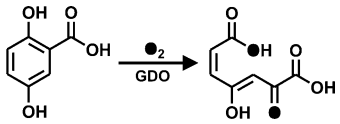

Scheme 1. Reaction catalyzed by GDO.

pyruvate is further degraded by direct hydrolysis to maleate and pyruvate or undergoes isomerization to form fumaryl pyruvate which hydrolyzes to form fumarate and pyruvate, the central metabolites of the Krebs cycle.[11,12] Other enzymes related to GDO involved in the degradation of aromatic compounds, such as 1-hydroxy-2-naphthoate 1,2-dioxygenase (HNDO) and salicylate 1,2-dioxygenase (SDO), cleave the aromatic ring of their substrates.[1] Although GDO displays sequence similarity to HNDO and SDO, salicylate and 1-hydroxy-2-napththoate are not active substrates of GDO.[3,6] However, the relative activity of GDO against 1,4-dihydroxy-2-naphthoate is high.[13] These data indicate that GDO is specific to dihydroxylated substrates. On the contrary, gentisate and 1-hydroxy-2-napththoate are cleaved by SDO. Therefore SDO is a GDO which can cleave the aromatic ring of monohydroxylated substrates.[14]

The crystal structure of GDO from *Escherichia coli* exhibits significant structural similarity to other bicupin proteins and is a homotetramer containing one ferrous ion per tetramer at the active site of the enzyme.[15] The X-ray structure of GDO from *Silicibacter Pomeroyi* reveals that each mononuclear iron is coordinated by three histidine residues and three labile water molecules.[16] Substrate gentisate and dioxygen coordinate to the iron center by replacing the solvent molecules to initiate the C–C bond cleavage reaction.

Although there are several reports on the characterization and biochemical studies of this enzyme,[3,5,10,13,17] functional model of GDO exhibiting the oxidative C–C bond cleavage of gentisate has not been developed yet. Moreover, the mechanistic details of this enzymatic reaction remain unexplored. Thus, to develop an understanding of the reaction catalyzed by GDO, we have examined the reactivity of a biomimetic iron(II) complex [(Tp^{Ph2})Fe^{II}(DHN-H)] (**1**; Tp^{Ph2} = hydrotris(3,5-diphenylpyrazole-1-yl)borate and DHN-H_2 = 1,4-dihydroxy-2-naphthoic acid) toward dioxygen. The high activity of 1,4-dihydroxy-2-naphthoate against GDO was the reason for our choice of the substrate/co-ligand.

The iron(II) complex **1** was isolated from the reaction of KTp^{Ph2} and iron(II) perchlorate hydrate with monoanionic 1,4-dihydroxy-2-naphthoic acid in methanol at room temperature (Experimental Section in the Supporting Information). The optical spectrum of **1** is dominated by one intense absorption band at 340 nm (Figure S1 in the Supporting Information). Complex **1** displays proton resonances between 60 ppm and −10 ppm in the ^{1}H NMR spectrum (Figure S2) and exhibits room temperature magnetic moment value of 5.0 μ_B. The X-ray single crystal structure of **1**·CH_2Cl_2 confirms the formation of a neutral mononuclear iron complex. The iron center is coordinated by three nitrogen donors from the supporting ligand (Tp^{Ph2}) and by two oxygen donors from the carboxylate group of 1,4-dihydroxy-2-naphthoate co-ligand (DHN-H; Figure 1). The iron–nitrogen bonds in the range of 2.047(2)–2.146(1) Å are in good agreement with the reported high-spin iron(II) complexes of the Tp^{Ph2} ligand.[18,19] The monoanionic DHN-H shows an asymmetric bidentate bind-

[*] R. Rahaman, Dr. B. Chakraborty, Prof. T. K. Paine
Department of Inorganic Chemistry
Indian Association for the Cultivation of Science
2A & 2B Raja S. C. Mullick Road, Jadavpur, Kolkata-700032 (India)
E-mail: ictkp@iacs.res.in

Supporting information for this article can be found under: http://dx.doi.org/10.1002/anie.201607044.

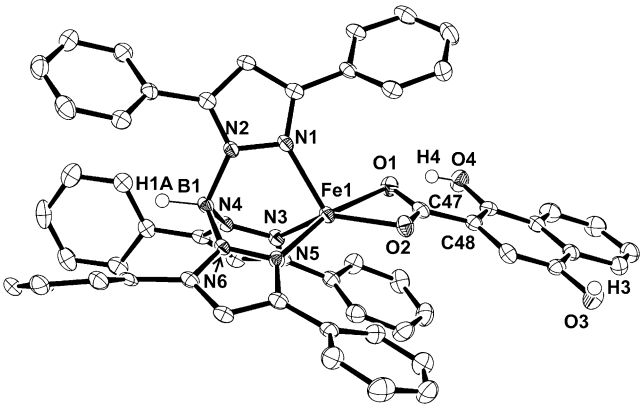

Figure 1. ORTEP plot of **1**·CH_2Cl_2 thermal ellipsoids set at 55% probability. The solvent molecule and all the hydrogen atoms except those on B1, O3, and O4 have been omitted for clarity. Selected bond lengths [Å] and angles [°]: Fe1–O1 2.414(2), Fe1–O2 1.998(2), Fe1–N1 2.081(2), Fe1–N3 2.047(2), Fe1–N5 2.146(2), C47–O1 1.254(3), C47–O2 1.298(3), C47–C48 1.470(3); N1-Fe1-O2 126.71(7), N3-Fe1-O2 133.63(7), N5-Fe1-O2 113.46(8), N1-Fe1-O1 98.95(7), N3-Fe1-O1 92.63(7), N5-Fe1-O1 166.61(7), N1-Fe1-N3 90.59(8), N3-Fe1-N5 85.95-(7), O1-Fe1-O2 58.80(7).

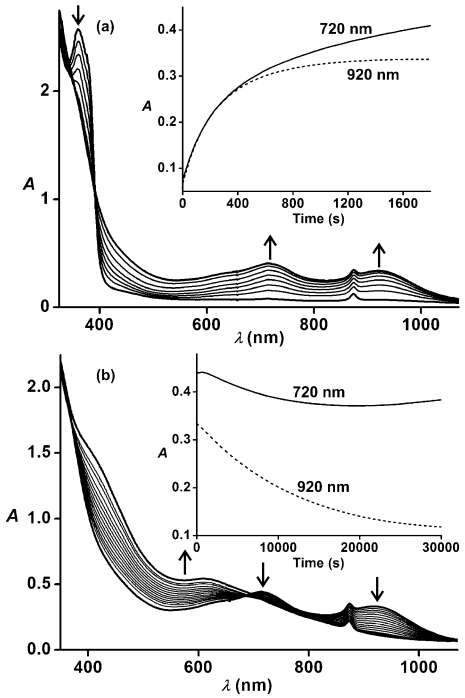

Figure 2. Optical spectral changes with time during the reaction of **1** (0.5 mM in benzene) with dioxygen at 298 K. a) reaction during the first 30 min, and b) reaction for the next 8 h. Insets: Plots of absorbance versus time.

ing mode (κ^2) with the Fe1−O1 and Fe1−O2 bonds of 2.414(2) and 1.998(2) Å, respectively. The *ortho* hydroxy group of DHN-H remains non-coordinated. The binding modes of the supporting ligand and the co-ligand enforce a distorted trigonal bipyramidal coordination geometry ($\tau = 0.55$)[20] at the iron center. One of the pyrazole nitrogen atoms (N5) of Tp^{Ph2} and the carboxyl oxygen atom (O1) occupy the axial position with the N5-Fe1-O1 angles of 166.61(7)°. Solid-state packing of **1** reveals three hydrogen-bonding interactions in which one of the coordinated carboxylate oxygen atoms (O1) is intra-molecularly H-bonded with the OH group, and the other two oxygen atoms that is, O2 and O3 are inter-molecularly H-bonded.

The geometry of **1** could not be optimized by DFT calculation. However, optimization of an analogous model complex [(Tp^{Me2})Fe^{II}(DHN-H)] (**1′**) was performed using the atomic coordinates obtained from the crystal structure of **1**. The calculated bond parameters (Table S1) of the high-spin iron(II) complex **1′** ($S = 2$) are in good agreement with those obtained experimentally for **1**. From the Mulliken spin-density plot of the optimized geometry (Figure S3), it is observed that 94% of the total electron density is localized on the iron center, 2% on the 1,4-dihydroxy-2-naphthoate ring and the rest on the supporting Tp^{Ph2} ligand (Table S2).

Complex **1** reacts with O_2 in dry benzene at room temperature within 30 min during which the colorless solution turns deep green. In the reaction, the absorption band at 340 nm disappears and two new charge-transfer (CT) bands at 720 nm and 920 nm appear following a pseudo-first order rate (Figure 2a). Similar spectral changes are observed during the reactions of iron(II) catecholate and iron(II) 2-aminophenolate complexes of nitrogen-donor polydentate ligands with oxygen.[21–25] By analogy to iron(III) catecholate/2-amidophenolate compounds, the bands at 720 nm and 920 nm could be assigned as the 1,4-dihydroxy-2-naphthoate (DHN)-to-iron-(III) CT transitions. The ESI-mass spectrum of this deep-green solution exhibits an ion peak at m/z 725.09 with the isotope distribution pattern calculated for [(Tp^{Ph2})Fe]$^+$ (Figure S4). In the X-band EPR spectrum collected at 77 K, a rhombic signal at $g = 4.2$ for a high-spin iron(III) species is observed after 30 min of the reaction between **1** and O_2 (Figure S4).

The reaction of **1** with 1 equivalent of 2,4,6-tri-*tert*-butylphenoxyl radical (one-electron oxidant) results in the formation of a green solution (Figure S5) that exhibits spectral patterns very similar to that of the oxidized solution (**1^{Ox}**) after the reaction between of **1** and O_2 for 30 min. Several attempts to isolate single crystals of **1^{Ox}** were unsuccessful. Therefore, DFT calculations were conducted to optimize the geometry of [(Tp^{Me2})Fe^{III}(DHN)] (**1′^{Ox}**) with the $S = 5/2$ spin state (Table S3). TD-DFT calculation (Table S4) of the optimized geometry of **1′^{Ox}** exhibits three major absorption bands in the 300–1200 nm region (Figure S6) that are well correlated with the experimental data. Note that the calculated optical spectra of **1′^{Ox}** with $S = 3/2$ and 1/2 spin state do not show any similarity to the experimental spectrum of **1^{Ox}**. All these results establish the formation of an iron(III)-1,4-dihydroxy-2-naphthoate (DHN) species (**1^{Ox}**) in the first step by one-electron oxidation of **1** in reaction with dioxygen. A sufficient electron density is observed on 1,4-dihydroxy-2-naphthoate (DHN) ring (13.9%) (Figure S3 and Table S2) in the spin-density plot of [(Tp^{Me2})Fe^{III}(DHN)] which could facilitate further reaction with dioxygen. In the next step of the reaction, the CT bands at 720 nm and 920 nm decay slowly over 8 h (Figure 2b). The

decay of the CT bands suggests the oxidation of metal-bound naphthoate. Similar spectral change is observed upon exposure of a benzene solution of $\mathbf{1^{Ox}}$, prepared in situ by mixing **1** and 1 equivalent of 2,4,6-tri-*tert*-butylphenoxyl radical, to dioxygen. Reactions at different concentrations of the complex reveal the reaction to be first order in iron complex supporting the involvement of a single metal center during the reaction pathway.

The product derived from 1,4-dihydroxy-2-naphthoic acid was isolated from the oxidized solution of **1** by acidic work-up and was analyzed by ^{1}H NMR spectroscopy. In time-dependent ^{1}H NMR spectra, the proton signals of 1,4-dihydroxy-2-naphthoic acid slowly disappear with time with the formation of new resonance signals (Figure S7). The ESI-mass spectrum of the organic product after treatment with diazomethane exhibits molecular ion peak at *m*/*z* 265.10 with the isotope distribution patterns calculated for $[M+H]^+$, where $M=$ dimethyl-2′-carboxy-4-hydroxybenzalpyruvate (Figure 3). In addition to the molecular ion peak, two ion fragments are observed at *m*/*z* 251.10 and 235.10 attributable to $[(M-CH_3)+H]^+$ and $[(M-2CH_3)+H]^+$, respectively (Figure 3a). The ESI-mass spectrum of the solution after the reaction between **1** and $^{18}O_2$ in dry benzene displays molecular ion peak at *m*/*z* 237.10 (15% ^{18}O incorporation) and *m*/*z* 239.10 (53% ^{18}O incorporation) indicating the incorporation of both single- and double-labelled oxygen atom into the dimethyl ester of 2′-carboxy-4-hydroxybenzalpyruvic acid (Figure 3b). The labelling experiment with $^{16}O_2$ and $H_2{}^{18}O$ shows about 10% incorporation of one labelled oxygen atom from water into the cleavage product suggesting the exchange of water with an iron–oxygen intermediate in the reaction pathway (Figure S8). No incorporation of labelled oxygen from water is observed when dimethyl-2′-carboxy-4-hydroxybenzalpyruvate and $H_2{}^{18}O$ are stirred together for 4 h at room temperature. Labelling experiments with a GDO gene from a halophilic *martelella* strain have indicated that two ^{18}O atoms were incorporated into maleylpyruvate product in the reaction with $H_2{}^{18}O$ and $^{18}O_2$.[10] Thus the formation of 2′-carboxy-4-hydroxybenzalpyruvic acid from 1,4-dihydroxy-2-naphthoic acid on the iron complex functionally mimics the reaction catalyzed by gentisate-1,2-dioxygenase (Scheme 2).

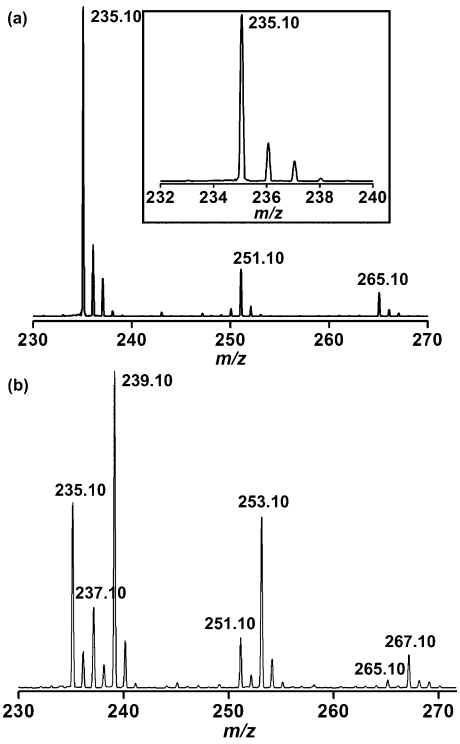

Figure 3. ESI-mass spectra (positive-ion mode in acetonitrile) of (the dimethyl ester of) 2′-carboxy-4-hydroxybenzalpyruvic acid obtained in the reaction of **1** with a) $^{16}O_2$ and b) $^{18}O_2$.

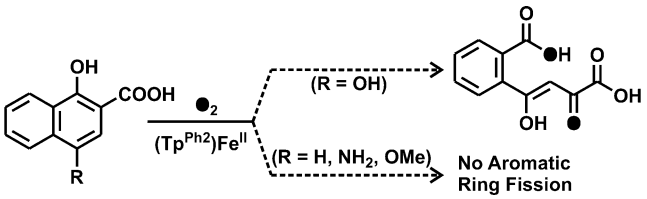

Scheme 2. Reactivity of the $(Tp^{Ph2})Fe^{II}$ complex toward different substrates.

Although the ring-cleavage product (as dimethyl ester of 2′-carboxy-4-hydroxybenzalpyruvic acid) was detected by ESI-MS, the same could not be characterized unambiguously by ^{1}H NMR spectroscopy because of the presence of a number of peaks from pyrazole. Therefore, the cleavage product was purified by preparative thin-layer chromatography (TLC). Although the pyrazole could be removed from the mixture, the number of peaks, and their position and integration values in the ^{1}H NMR spectrum indicate that dimethyl-2′-carboxy-4-hydroxybenzalpyruvate undergoes transformation to the corresponding lactone derivative along with some unidentified decomposition product during the purification process (Figure 4, and Scheme S1). The formation of lactone species is also confirmed by ^{13}C NMR,

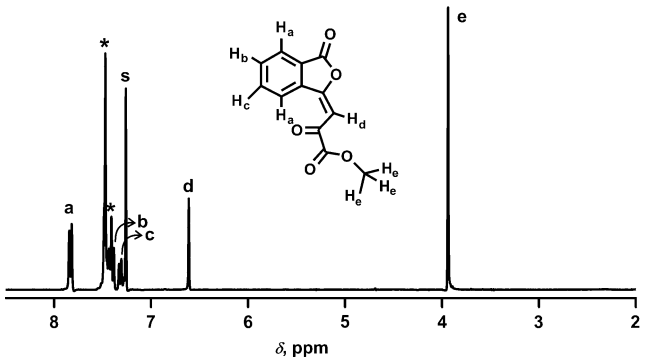

Figure 4. ^{1}H NMR (300 MHz, $CDCl_3$, 298 K) spectrum of the lactone form of dimethyl-2′-carboxy-4-hydroxybenzalpyruvate. The peaks marked with * represent some unidentified decomposition product(s). The "s" marked peak originates from $CHCl_3$.

HSQC, and COSY spectroscopy (Figures S9–11). It is important to note that the ring-cleavage product decays slowly upon it being allowed to stand in solution (Figure S12).

The reactivity of other substrates, such as gentisate, 4-methyl salicylate, 1-hydroxy-2-naphthoate, and 5-methoxysalicylate, with dioxygen and the $(Tp^{Ph2})Fe^{II}$ complex was also investigated. The iron(II) gentisate complex $[(Tp^{Ph2})Fe^{II}(GN)]$ (**2**) also reacts with dioxygen to oxidize the metal-coordinated gentisate (Figure S13). However, the ring-cleavage product of gentisate, being unstable, could not be isolated for further characterization.[3] On the contrary, the other complexes, $[(Tp^{Ph2})Fe^{II}(4\text{-MSA})]$ (**3**), $[(Tp^{Ph2})Fe^{II}(HNA)]$ (**4**) and $[(Tp^{Ph2})Fe^{II}(5\text{-OMeSA})]$ (**5**) (where, 4-MSA = 4-methylsalicylate, HNA = 1-hydroxy-2-naphthoate, and 5-OMeSA = 5-methoxysalicylate; Experimental Section in Supporting Information) are unreactive toward dioxygen under similar experimental conditions. These results are in line with the substrates selectivity exhibited by GDO. Therefore, the presence of an hydroxy group in the 4 position on the aromatic ring is crucial for the oxygen-dependent C–C bond-cleavage reaction (Scheme 2). The iron(II)-5-aminosalicylate complex, $[(Tp^{Ph2})Fe^{II}(5\text{-ASA})]$ (**6**; Experimental Section in Supporting Information) in which the OH group of gentisate is replaced by a NH_2 group, reacts with dioxygen to form an iron(III) species (Figure S14). Although 5-aminosalicylate has been reported to be an alternate substrate of GDO,[3] the 5-aminosalicylaye complex **5** does not undergo C–C bond cleavage pathway further supporting the electronic role played by the *para*-hydroxy group in directing the reactivity.

The experimental observations discussed above provide a basis to propose the mechanism of the C–C cleavage reaction (Scheme 3). In the first step, the iron(II) 1,4-dihydroxy-2-naphthoate complex (**1**) reacts rapidly with dioxygen to generate the corresponding iron(III) species ($\mathbf{1^{Ox}}$) with concomitant loss of a proton from the 2-hydroxy group. Owing to extended conjugation and sufficient electron density on the naphthoate ring, the iron(III) 1,4-dihydroxy-2-naphthoate complex reacts with dioxygen to form an iron(III) superoxo radical intermediate through mixing with the low-lying excited state from iron(II) carboxysemiquinonato radical species (**I**). Fiedler's group has recently shown that mononuclear iron(III) 2-(1-methylbenzimidazol-2-yl)hydroquinonate complexes of tridentate facial N_3 ligands undergo deprotonation to generate the corresponding iron(II) semiquionate radical species.[26] The superoxide radical (**II**) can attack the C1 carbon of the carboxysemiquinonato group to form an alkylperoxide intermediate (**III**).[27] The *para*-hydroxy group on the aromatic ring then participates in directing the heterolytic O–O cleavage of the alkylperoxo intermediate (**III**) through Criegee type rearrangement to form an anhydride intermediate (**IV**). The resulting metal-coordinated hydroxide, which can exchange with water, finally participates in the hydrolysis of the anhydride species to afford the ring cleavage product, 2′-carboxy-4-hydroxybenzalpyruvic acid. The mechanism is reminiscent of the extradiol cleaving catechol and aminophenol cleaving dioxygenases.

In conclusion, we have synthesized and structurally characterized a biomimetic iron(II) complex of a tridentate facial nitrogen donor ligand. The model iron(II) complex has been shown to react with dioxygen and cleave the C–C bond of 1,4-dihydroxy-2-naphthoate between the hydroxy and carboxylate group. In the C–C bond cleavage reaction, two oxygen atoms from dioxygen are incorporated into the cleavage product. Additionally, partial incorporation of labelled oxygen atom from water is also observed in the reaction pathway. The presence of the *para*-hydroxy group of gentisate/1,4-dihydroxy-2-naphthoate plays a crucial role in directing the oxidative C–C bond cleavage reaction. Complex **1** thus represents the first functional model of gentisate-1,2-dioxygenase. The C–C bond cleavage reaction of gentisate-type substrate by the iron complex reported in this work would provide useful information toward developing bioinspired oxidation catalyst for degradation of aromatic pollutants.

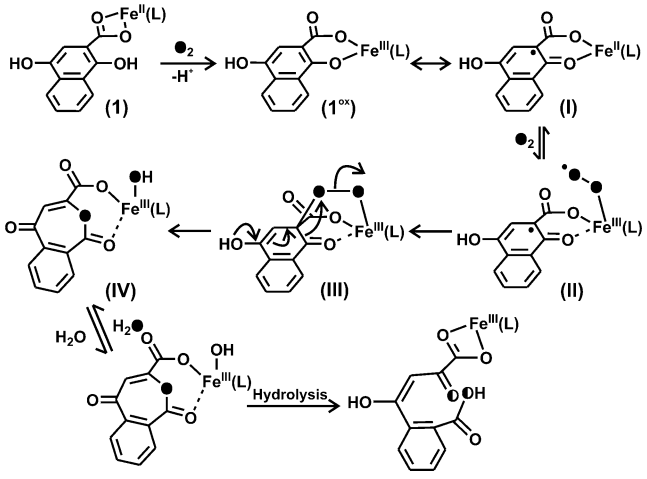

Scheme 3. Proposed reaction pathway for the C–C bond cleavage reaction of gentisate-type substrate on **1**. See text for details.

Acknowledgements

T.K.P. acknowledges the Council of Scientific and Industrial Research (CSIR) for the financial support (Project File No. 01(2776)/14/EMR-II). RR thanks CSIR for a research fellowship. We thank Mr. Sayantan Das for his help with NMR spectroscopic studies.

Keywords: biomimetic models · C–C bond cleavage · dioxygen · gentisate · iron complexes

How to cite: *Angew. Chem. Int. Ed.* **2016**, *55*, 13838–13842
Angew. Chem. **2016**, *128*, 14042–14046

[1] S. Fetzner, *Appl. Environ. Microbiol.* **2012**, *78*, 2505.
[2] F. H. Vaillancourt, J. T. Bolin, L. D. Eltis, *Crit. Rev. Biochem. Mol. Biol.* **2006**, *41*, 241.
[3] M. R. Harpel, J. D. Lipscomb, *J. Biol. Chem.* **1990**, *265*, 22187.
[4] T.-c. Feng, C.-z. Cui, F. Dong, Y.-y. Feng, Y.-d. Liu, X.-m. Yang, *J. Appl. Microbiol.* **2012**, *113*, 779.
[5] Y. Feng, H. E. Khoo, C. L. Poh, *Appl. Environ. Microbiol.* **1999**, *65*, 946.

[6] M. R. Harpel, J. D. Lipscomb, *J. Biol. Chem.* **1990**, *265*, 6301.
[7] J. Werwath, H. A. Arfmann, D. H. Pieper, K. N. Timmis, R. Wittich, *J. Bacteriol.* **1998**, *180*, 4171.
[8] S. Luo, D. Q. Liu, H. Liu, N. Y. Zhou, *Microbiol. Res.* **2006**, *161*, 138.
[9] D. J. Fairley, G. Wang, C. Rensing, I. L. Pepper, M. J. Larkin, *Appl. Microbiol. Biotechnol.* **2006**, *73*, 691.
[10] L. Huang, H. Hu, H. Tang, Y. Liu, P. Xu, J. Shi, K. Lin, Q. Luo, C. Cui, *Sci. Rep.* **2015**, *5*, 14307.
[11] R. C. Bayly, P. J. Chapman, S. Dagley, D. Di Berardino, *J. Bacteriol.* **1980**, *143*, 70.
[12] D. J. Hopper, P. J. Chapman, S. Dagley, *Biochem. J.* **1968**, *110*, 798.
[13] S.-i. Hirano, M. Morikawa, K. Takano, T. Imanaka, S. Kanaya, *Biosci. Biotechnol. Biochem.* **2007**, *71*, 192.
[14] M. Ferraroni, I. Matera, S. Bürger, S. Reichert, L. Steimer, A. Scozzafava, A. Stolz, F. Briganti, *FEBS J.* **2013**, *280*, 1643.
[15] M. A. Adams, V. K. Singh, B. O. Keller, Z. Jia, *Mol. Microbiol.* **2006**, *61*, 1469.
[16] J. Chen, W. Li, M. Wang, G. Zhu, D. Liu, F. Sun, N. Hao, X. Li, Z. Rao, X. C. Zhang, *Protein Sci.* **2008**, *17*, 1362.
[17] J.-P. Hintner, C. Lechner, U. Riegert, A. E. Kuhm, T. Storm, T. Reemtsma, A. Stolz, *J. Bacteriol.* **2001**, *183*, 6936.
[18] S. Paria, L. Que, Jr., T. K. Paine, *Angew. Chem. Int. Ed.* **2011**, *50*, 11129; *Angew. Chem.* **2011**, *123*, 11325.
[19] M. P. Mehn, K. Fujisawa, E. L. Hegg, L. Que, Jr., *J. Am. Chem. Soc.* **2003**, *125*, 7828.
[20] A. W. Addison, T. N. Rao, J. Reedijk, J. van Rijn, G. C. Verschoor, *J. Chem. Soc. Dalton Trans.* **1984**, 1349.
[21] D.-H. Jo, Y.-M. Chiou, L. Que, Jr., *Inorg. Chem.* **2001**, *40*, 3181.
[22] T. Ogihara, S. Hikichi, M. Akita, Y. Moro-oka, *Inorg. Chem.* **1998**, *37*, 2614.
[23] B. Chakraborty, T. K. Paine, *Angew. Chem. Int. Ed.* **2013**, *52*, 920; *Angew. Chem.* **2013**, *125*, 954.
[24] B. Chakraborty, S. Bhunya, A. Paul, T. K. Paine, *Inorg. Chem.* **2014**, *53*, 4899.
[25] S. Chatterjee, T. K. Paine, *Inorg. Chem.* **2015**, *54*, 1720.
[26] A. E. Baum, S. V. Lindeman, A. T. Fiedler, *Eur. J. Inorg. Chem.* **2016**, 2455.
[27] G. J. Christian, S. Ye, F. Neese, *Chem. Sci.* **2012**, *3*, 1600.

Received: July 20, 2016
Revised: August 30, 2016
Published online: September 28, 2016

